Journal of Molecular Catalysis A: Chemical 305 (2009) 161–169

Contents lists available at ScienceDirect

Journal of Molecular Catalysis A: Chemical

journal homepage: www.elsevier.com/locate/molcata

Selective blocking of active sites on supported gold catalysts by adsorbed thiols and its effect on the catalytic behavior: A combined experimental and theoretical study

Peter Haider, Atsushi Urakawa, Erik Schmidt, Alfons Baiker*

Department of Chemistry and Applied Biosciences, ETH Zurich, Hönggerberg, HCI, CH-8093 Zurich, Switzerland

ARTICLE INFO

Article history:
Available online 3 March 2009

This paper is dedicated to the memory of Professor Eric Derouane.

Keywords:
Gold
Hydrogenation of ketopantolactone
Oxidation of benzyl alcohol
Selective poisoning
Site blocking
Thiols

ABSTRACT

Selective blocking (poisoning) of catalytic active sites of gold catalysts, CeO_2 and TiO_2 supported Au colloids (2.1 and 6.9 nm), was investigated in the aerobic oxidation of benzyl alcohol as well as in the hydrogenation of ketopantolactone by adding various amounts of two chemically distinct thiols with different functionalities (n-octadecanethiol, ODT, and mercaptoacetic acid, MAA). There were clear trends in their poisoning behaviors, independent of the type of support and Au particle size. ODT poisoned the catalyst in the oxidation reaction much stronger than MAA. In contrast, MAA was a stronger poisoning agent in the hydrogenation reaction. The characteristics of supported Au particles and the nature of thiol adsorption were investigated by Attenuated Total Reflection Infrared (ATR-IR) spectroscopy, TEM, thermogravimetric desorption and DFT calculations. Based on the adsorption characteristics of two thiols derived from the combined experimental and theoretical study, it is suggested that C=O hydrogenation of ketopantolactone occurs preferentially at low coordination sites such as corners and edges, which are more dominant in small clusters, while oxidation seems to be favored on extended active sites as prevailing on larger Au clusters.

1. Introduction

Au has received considerable attention in the catalysis community, as reflected in several reviews [1–7]. The most frequently studied reaction on supported Au nanoparticles is the oxidation of CO, which exhibits a strong dependence on the particle size: small particles up to a mean diameter of ≈2–3 nm show far superior activity compared to larger analogues due to the higher relative concentration of low coordinated Au sites [8–16]. However, larger Au particles are known to catalyze various reactions as well, e.g. the amination of CO [17] and the oxidation of amines [18] and styrene [19] as well as the oxidation of alcohols where larger particles (>4–5 nm) were found to be highly active [20–26].

Recently, we [27,28] and another group [29] have independently reported a similar correlation between the catalytic activity and particle size in the Au catalyzed oxidation of alcohols. Medium sized particles in a range of 4–7 nm were more active than smaller and larger particles in these reactions [27–29]. Larger Au particles have also been found to be active, e.g. in the oxidation of glycerol and ethylene glycol [30,31]. For Pt (3.2 nm, [32]) and Pd (3.6–4.3 nm, [33]), a similar trend has been observed, meaning that medium sized particles showed higher conversion compared to smaller ones in the aerobic oxidation of alcohols. The size can drastically alter the electronic and structural properties of metal particles; several critical properties for catalysis, e.g. binding strength of substrates, exposed crystal faces, relative amount of low coordinated edge and corner atoms, particle height, and the perimeter between the particles and support, change with particle size. Such properties as well as kinks, steps and adatoms are known to influence activity and selectivity of surface catalyzed reactions [9,34–41].

In the present contribution, the adsorption of two different thiols (n-octadecanethiol (ODT) and mercaptoacetic acid (MAA)) on small Au colloids (2.1 nm) and larger analogues (6.9 nm) supported on CeO_2 and TiO_2 was employed to study the effect of specific blocking of surface sites on the catalytic behavior of the gold-catalyzed aerobic oxidation of benzyl alcohol and the hydrogenation of ketopantolactone. *In situ* ATR-IR, thermogravimetric desorption experiments and DFT calculations were performed to gain some insight into the adsorption of the thiols on the supported gold particles and to trace the remarkably different blocking effects of exposed gold sites by these thiols in the two test reactions.

* Corresponding author. Fax: +41 44 632 11 63.
E-mail address: baiker@chem.ethz.ch (A. Baiker).

1381-1169/$ – see front matter © 2009 Elsevier B.V. All rights reserved.
doi:10.1016/j.molcata.2009.02.025

2. Experimental

2.1. Materials

Commercially available support materials were used: CeO_2 was purchased from MCT Microcoating Technologies and TiO_2 (P25) was purchased from Degussa. Chemicals used were $H[AuCl_4]\cdot 3H_2O$ (99.99% ACS (metals basis), Alfa Aesar), tetrakis(hydroxy-methyl) phosphonium chloride (THPC, 80% in water, Fluka), $CHCl_3$ (HPLC grade, Acros), toluene (HPLC grade, Acros), n-octadecanethiol (ODT, 98%, Aldrich), mercaptoacetic acid (MAA, 98%, Fluka), benzyl alcohol (>99%, Fluka), benzaldehyde (99.5%, Acros), dihydro-4,4-dimethyl-2,3-furandione (99%, Roche). The gases used were Ar 4.8, O_2 5.0, He 5.0 and H_2 5.0 (PanGAS).

2.2. Catalysts preparation

Au/CeO_2 and Au/TiO_2 catalysts were prepared as previously described [28,42,43]. In brief, for the synthesis of 10 mg Au colloid (mean diameter ≈2.1 nm), 1.5 ml of a freshly prepared 0.2 mol/l NaOH solution and 1 ml of a freshly prepared tetrakis(hydroxy-methyl)phosphonium chloride (THPC) solution (1.2 ml in 100 ml H_2O) were mixed with 45.5 ml deionized water and stirred for 2 min. Subsequently, 2 ml of a stock solution containing 1 g of $H[AuCl_4]\cdot 3H_2O$ in 100 ml H_2O was added, resulting in a brown mixture. The mixture was added to the acidified solution (pH 2) of the support, stirred for 5–10 min, filtered and washed exhaustively with deionized water. The material was dried 18 h at 80 °C in static air. The alteration of the particle size was achieved by variation of the amounts of NaOH, THPC and $H[AuCl_4]$ as described in [28]. The theoretical weight loading of all catalysts used for oxidation and hydrogenation reactions was 1 wt%.

2.3. Characterization of size and shape of gold particles

For the analysis of the particle size distribution, the detection limit is a crucial parameter as shown in a recent publication elucidating the role of small Au clusters with a diameter of 0.5 nm and smaller to CO oxidation catalysis [44]. In the present contribution, the transmission electron microscopy was conducted using a Tecnai F30 FEI (field emission cathode, operated at 300 keV) with a point resolution of <2 Å. This instrumentation is capable of detecting even very small metal particles (<1 nm) by Z contrast. The particle size distribution of the materials used has already been reported elsewhere [28]: for the two colloids, 338 and 196 particles were counted leading to mean particles sizes of 2.0 nm and 6.9 nm, respectively (standard deviations 0.8 nm and 3.6 nm, respectively). The materials were analyzed by means of XPS [28] and the absence of Na and P was confirmed.

2.4. Catalytic tests

The hydrogenation reactions were performed in a 50 ml autoclave at room temperature and 50 bar. 100 ± 0.2 mg of the specified catalyst (1 wt% Au) was mixed with 60 ± 1 mg ketopantolactone leading to a substrate/Au_{Total} ratio (molar ratio calculated from the number of substrate molecules and the total number of Au atoms) of 92. Subsequently, toluene (dried with molar sieve 4 Å) or – if desired – a solution containing the appropriate amount of the blocking (poisoning) agent (ODT or MAA) in toluene was added as a solvent. The slurry was stirred with a magnetic stirrer (750 rpm) and pressurized with H_2 (50 bar). In standard experiments the reaction was performed for 4 h to ensure incomplete conversion of ketopantolatone allowing for a comparison of the activity of the different catalysts. The reaction mixtures were filtered, diluted with ethyl acetate and subsequently analyzed by means of gas chromatography on a Thermo Finnigan Trace 2000 using a CP-Chirasil-Dex CB capillary column and a FID detector.

The aerobic oxidation of benzyl alcohol was carried out in a 50 ml 2-neck round glass flask at 100 °C for 3 h using 100 ± 1 mg of each catalyst and 700 μl benzyl alcohol in 5 ml toluene. Oxygen (50 ml/min) was bubbled through the vigorously stirred solution at atmospheric pressure. A cooler was placed on top to avoid fatal loss of involved materials, resulting in an average error of the mass balance of the alcohol, aldehyde/ketone and ester of $2.01 \pm 1.59\%$ determined by comparing the areas of all substrates and products with an inert internal standard added (tetradecane). Samples were taken during and at the end of every experiment, filtered and diluted with isopropanol for subsequent gas chromatographic analysis (Thermo Quest Trace 2000 employing a HP-FFAP capillary column and FID detector).

2.5. ATR-IR investigations

6 ± 0.1 mg of the Au/CeO_2 and Au/TiO_2 catalysts (5 wt% Au) was suspended in 0.8 ml water and stirred for at least 30 min. Subsequently, the slurry was placed on the Internal Reflection Element (IRE) and the water was evaporated in a vacuum oven at 40 °C and 100 mbar overnight. ZnSe crystals (45°, 50 mm × 20 mm × 2 mm, Komlas) were used as IREs.

The catalyst was analyzed in flow-through mode using solutions of 1 mM concentration of ODT and MAA. Note that the IRE itself was pretreated with the corresponding thiol prior to the deposition of the catalyst particles. 5 wt% Au catalysts were employed for the ATR-IR investigations to improve the signal to noise ratio, although an identical trend was confirmed employing 1 wt% Au catalysts used in the catalytic tests (see electronic support information for comparison).

The cell used for modulation experiments has been described in detail in [45]. All solutions were freshly prepared using dried solvents ($CHCl_3$, toluene). The corresponding liquids were saturated with the desired gases (Ar, O_2) for at least one hour in order to ensure a defined gas atmosphere before the experiment was started.

Unless stated otherwise, spectra were recorded averaging 200–300 scans (mirror velocity 80 kHz) on a Bruker IFS66/S and a Bruker Equinox 55 spectrometer equipped with a commercial ATR accessory (Optispec) using a resolution of 2 cm^{-1} for monitoring the adsorption of MAA and ODT. $CHCl_3$ was used as solvent due to the overlaps of the characteristic CH_2 stretching bands of ODT with those of toluene which was employed in the catalytic tests. The temperature was set to 25 °C. In order to bridge the gap between the conditions of the catalytic tests and *in situ* ATR-IR measurements described above, additional experiments were performed to validate the obtained results; spectra were recorded at 50 bar H_2 in a batch cell to mimic the hydrogenation reaction conditions and at 95 °C in a flow-through cell, using O_2-saturated toluene as the solvent to mimic the oxidation reaction conditions. Integration of the IR signals was performed using the software OPUS 5.0.

2.6. Thermogravimetric desorption

Thermogravimetric desorption experiments were conducted on a Netzsch STA 449 C thermoanalyzer. The desorbing gases were analyzed by a Thermostar (Pfeiffer Vacuum) mass spectrometer connected by heated stainless steel capillary. Prior to the experiments, samples (5 wt%) were treated with ODT or MAA solution in $CHCl_3$ for 1 h at room temperature. Each solution contained a 5-fold excess of the corresponding thiol, with respect to the total number of Au atoms, in order to ensure full coverage of the thiols on the Au surfaces as the desorption temperature could possibly be influenced by different coverage. Subsequently, the materials were

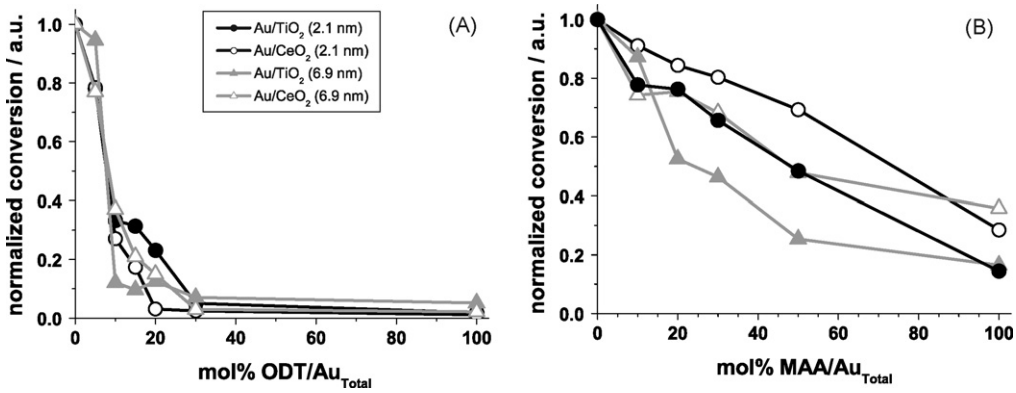

Fig. 1. Aerobic oxidation of benzyl alcohol. Poisoning effect of ODT (left, A) and MAA (right, B) on the catalytic activity of Au particles of 2.1 nm (circle, black) and 6.9 nm (triangle, gray) supported on TiO_2 (closed symbols) and CeO_2 (open symbols). Conditions: reactions were performed in 50 ml glass round flasks, 100 ± 1 mg catalyst (1 wt%), 100 °C, 3 h, 700 μl substrate, Oxygen flow: 50 ml/min.

washed with $CHCl_3$ and dried at room temperature. No trace of $CHCl_3$ was found by mass spectrometry. 100 mg of the sample was placed in the system under flowing He (50 ml/min). After equilibration of the balance and the MS signals, TPD experiments were performed in the flow of He starting from 30 °C and heating with 10 °C/min to 900 °C.

2.7. DFT calculations

Geometry optimization and single-point energy calculations were performed with the unrestricted B3PW91 hybrid functional [46,47] using Gaussian 03 [48]. A 6-311G(d,p) basis set was applied for all the atoms except Au. For Au, the LanL2DZ effective core potential (ECP) basis set was used [49]. A truncated tetrahedron Au cluster consisting of 37 atoms was used as the model of Au nanoparticles due to the various adsorption sites on the cluster. Au–Au distances were fixed at 2.8836 Å and only the structures of the adsorbed MAA thiolate were relaxed. The MAA thiolate adsorption energies at distinct adsorption sites were evaluated with and without considering basis set superposition error (BSSE) using counterpoise approximation [50]. All calculations were performed as an isolated system or complex without solvent effects.

3. Results

3.1. Oxidation of benzyl alcohol

Au/CeO_2 [51] and Au/TiO_2 [52] have been employed as catalysts for the oxidation of various aromatic and aliphatic alcohols. The Au catalysts supported on TiO_2 and CeO_2 showed a moderate catalytic activity and high selectivity in the liquid-phase oxidation of benzyl alcohol to benzaldehyde as reported in our previous study [28]. Independent of the type of support the activity exhibited clear maxima in the range of 2–7 nm gold particle size, while the selectivity was only weakly affected by the particle size. In this study, the same reaction was tested in the presence of the thiols, ODT and MAA, to investigate the blocking effect of Au surface sites on the catalytic activity. Gold particles of 2.1 and 6.9 nm size supported on TiO_2 and CeO_2 were used as catalysts. Fig. 1A and B show the normalized conversions of the reaction as a function of the concentrations of ODT and MAA, respectively. Note that the concentrations of thiol are shown relative to the total number of Au atoms. The trends of the conversion decrease, i.e. the poisoning effect, by ODT and MAA were greatly different. The ODT addition affected the catalytic activities in a similar manner for all the investigated catalysts despite the large differences in the particle size and the type of the support. Addition of 10 mol% ODT/Au_{Total} led to an almost complete loss of catalytic activity for both Au particle sizes (Fig. 1A). The absolute conversion values, TOFs and selectivity for the non-poisoned system are given in [28]. The influence of thiol addition on the selectivity was minor and not correlated to the amount of the thiols (not shown). The blocking effect by MAA on the reaction rate was far less pronounced compared to that of ODT; even the addition of 100 mol% MAA/Au_{Total} did not lead to a complete loss of oxidation activity (Fig. 1B). The Au particle size and the type of support had an effect on the poisoning by MAA. As a general trend the TiO_2 supported and larger Au particles were more sensitive to site-blocking than the CeO_2 supported and smaller Au particles.

3.2. Hydrogenation of ketopantolactone

Au catalysts show a high chemoselectivity towards the hydrogenation of C=O double bonds [53–56]. In the current study, the gold-catalyzed ketopantolactone hydrogenation was studied in the absence and presence of the site-blocking agents, ODT and MAA. No appreciable conversion was observed for CeO_2 supported catalysts, while TiO_2 supported catalysts showed reasonable activity with 100% selectivity to pantolactone, implying a remarkable support effect in the Au/CeO_2 catalytic system. The clarification of the origin of this support effect was beyond the scope of this work; therefore only the results obtained with the Au/TiO_2 catalysts are described and discussed hereafter for the hydrogenation reaction.

Table 1 and Fig. 2A and B show the effect of the presence of ODT and MAA on the hydrogenation of ketopantolactone for the 2.1 and 6.9 nm Au/TiO_2 catalysts. Similar to the previous site blocking experiments for the oxidation reaction, various molar amounts of

Table 1
Conversions (in %) and TOFs (h^{-1}, based on the total Au content) determined in the hydrogenation of ketopantolactone using 100 ± 0.2 mg Au/TiO_2 (1 wt%) and 60 ± 1 mg ketopantolactone at room temperature, hydrogen pressure was set to 50 bar, reaction time 4 h. The thiol/Au_{Total} ratio was set to 100%.

	Au/TiO_2 (2.1 nm) conversion (%)	Au/TiO_2 (2.1 nm) TOF (h^{-1})	Au/TiO_2 (6.9 nm) conversion (%)	Au/TiO_2 (6.9 nm) TOF (h^{-1})
No additives	61.6	14.21	15.1	3.48
$C_{18}H_{37}$-SH (ODT)	14.0[a]	3.23[a]	3.0[a]	0.69[a]
HS-CH_2-COOH (MAA)	4.0	0.92	1.5	0.35

[a] Leaching of Au observed.

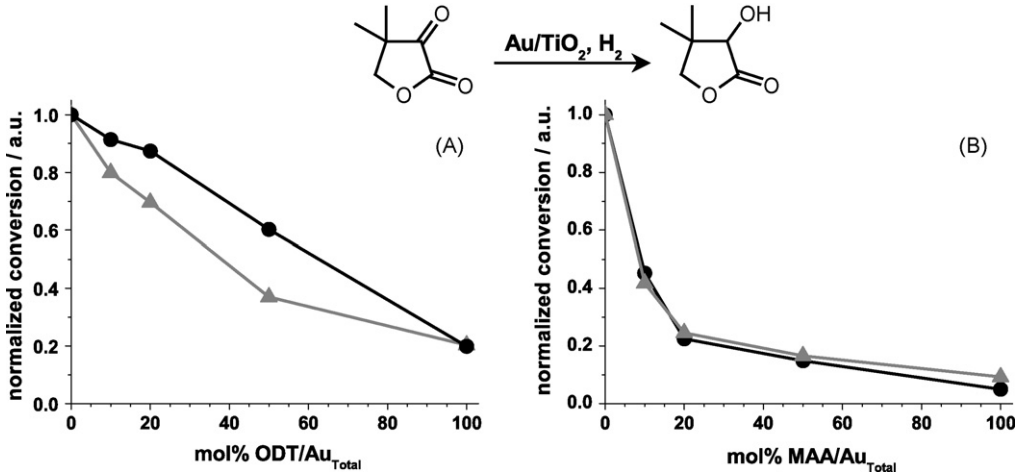

Fig. 2. Hydrogenation of ketopantolactone to pantolactone using Au/TiO_2. Poisoning effect of ODT (left, A) and MAA (right, B) on the catalytic activity of Au particles of 2.1 nm (circle, black) and 6.9 nm (triangle, gray) supported on TiO_2. Conditions: reactions were performed in an autoclave using glass inserts, 100 ± 1 mg catalyst (1 wt%), room temperature, 50 bar H_2, 4 h, 60 mg ketopantolactone.

ODT and MAA with respect to the *total* amount of Au present in the catalyst were added to the reaction mixture. Contrary to the oxidation reaction, the addition of MAA (Fig. 2B) led to more pronounced deactivation (blocking) of the catalyst than ODT addition (Fig. 2A). The catalysts were still active in the hydrogenation even when a large amount of ODT was present, in contrast to the almost full deactivation after 10 mol% ODT/Au_{Total} addition in the oxidation reaction. The blocking effect was not significantly affected by the Au particle size, and a stronger inhibition of the hydrogenation activity for MAA compared to ODT was also observed in the hydrogenation of benzaldehyde at 100 °C (see electronic support information). In order to elucidate the reasons for the striking differences observed in the poisoning tendency of the two thiols in the oxidation and hydrogenation reactions, the catalytic systems were subjected to a thorough characterization.

3.3. Morphology of gold particles

TEM pictures of the Au particles supported on TiO_2 are shown in Fig. 3. Two basic geometric patterns, cuboctahedron and truncated tetrahedron, were discernible. Fig. 3A depicts a particle, likely seen from the side that appears as a trapezoid. Fig. 3B shows a particle that exhibits triangular Au entities typical for a truncated tetrahedral shape. The Au particle shown in Fig. 3C is probably viewed from the top, appearing as a stretched, hexagonal shape. Assuming a cuboctahedron and a truncated tetrahedron particle shape of adsorbed Au particles of ca. 2.1 and 6.9 nm diameter (schemes in Fig. 4) this leads to respective dispersions of $\approx 55 \pm 3\%$ and $\approx 24 \pm 4\%$, depending on the symmetry settings [34,35]. Hence, under similar weight loading, the catalysts with the smaller Au particles possess a considerably larger Au surface area.

3.4. Octadecanethiol adsorption

Sulfur containing molecules like thiols are frequently used in the preparation of self-assembled monolayers (SAM) that have received great attention as evidenced by numerous articles ([57] and references therein). In the analysis of the adsorbed layer, the position of the resulting IR bands is conveniently utilized. The relative intensities of symmetric (ν_S) and asymmetric (ν_{AS}) stretching vibrations

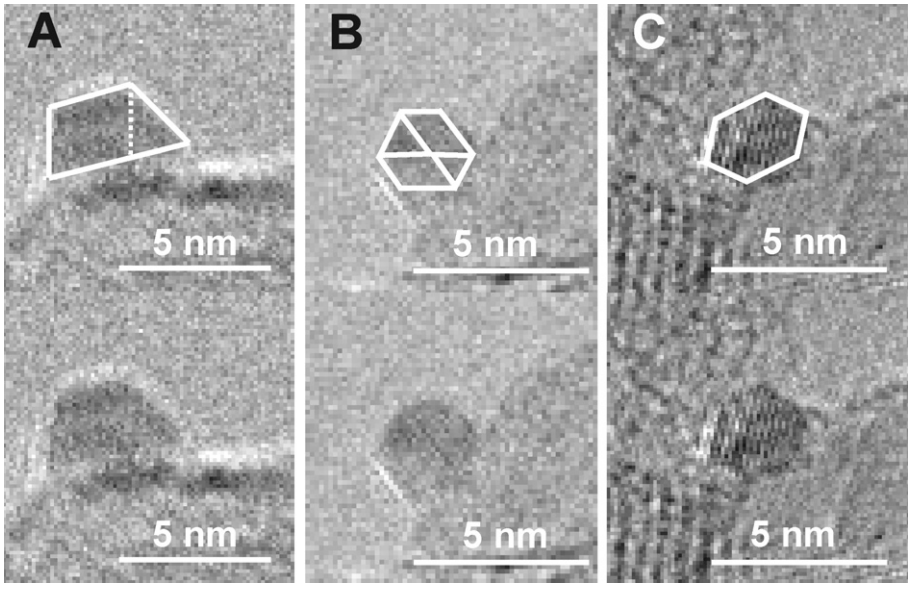

Fig. 3. TEM pictures of TiO_2 supported Au particles (mean diameter 2.1 nm) viewed from various angles. The white lines in the TEM pictures are drawn to guide the eye.

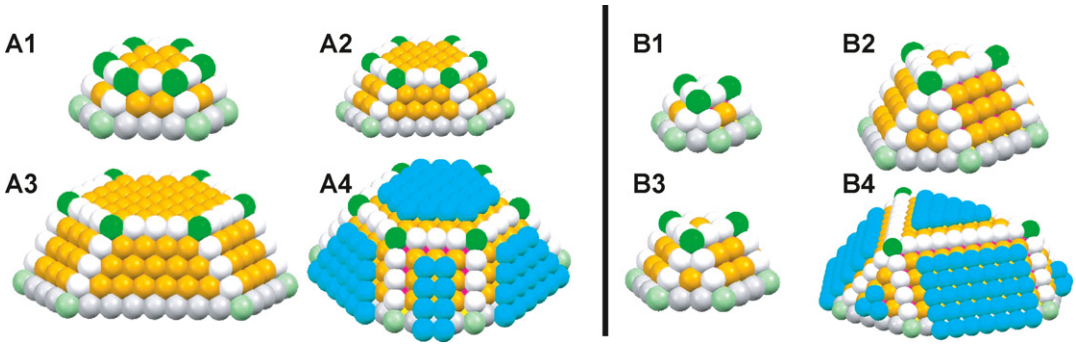

Fig. 4. Cartoon of adsorbed, flat Au particles adapting van Hardeveld-type structures to adsorbed particles [34,35]. Depicted are a cuboctahedron (section A) and truncated tetrahedral shape (section B). Atoms are colored according to: crystal facets/orange; edges/white; corner/green; corner in contact with the support/light green, edge in contact with the support/gray, adlayers forming B_5-sites/light blue. (For interpretation of the references to colour in this figure legend, the reader is referred to the web version of the article.)

of the methylene groups (CH_2) undergo a blueshift in the transition from crystalline-like (2918 and 2850 cm^{-1} for $\nu_{AS}(CH_2)$ and $\nu_S(CH_2)$) to liquid-like adsorbed layers (2928 and 2858 cm^{-1} for $\nu_{AS}(CH_2)$ and $\nu_S(CH_2)$) [58,59]. In ref. [60], the liquid-like layer structure was assigned to signals located as low as at 2924 and 2855 cm^{-1}. Various examples in literature indicate that the adsorption of small n-alkane thiols (n-octanethiol and shorter) leads to a less ordered and more irregular layer compared to longer analogues [60–63]. Also thiol adsorption on nanoparticles has been examined and a higher packing density compared to e.g. (1 1 1)-surfaces [64] is reported [65].

The adsorption behavior of ODT was monitored by *in situ* ATR-IR spectroscopy. The IR spectra of the characteristic C–H stretching region of ODT, recorded after passing an ODT solution for 1 h over the Au/TiO_2 catalyst deposited on the ATR-crystal, are shown in Fig. 5. An additional experiment of ODT adsorption on only TiO_2 evidenced a negligible adsorption of ODT on the support, clearly proving that the bands shown in Fig. 5 originate from the ODT molecules on the Au particles. After the ODT adsorption for 1 h the flow was switched to the neat solvent to study possible ODT desorption from the Au surface, but there was little change in the band intensities and positions. This indicates a strong adsorption of ODT on the supported Au particles. A summary of the observed band positions for the different Au catalysts is given in Table 2. The C—H stretching region shows bands at

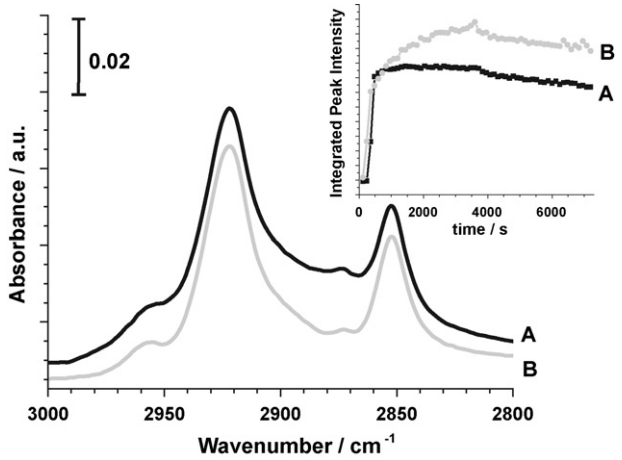

Fig. 5. ATR-IR spectra recorded after passing a 1 mM solution of ODT over the catalysts at 25 °C; Au/TiO_2 (2.1 nm) (black, A) and Au/TiO_2 (6.9 nm) (light gray, B). The inset shows the temporal profile of the $\nu_{AS}(CH_2)$ band of ODT during the experiment, mimicking the oxidation condition, where the O_2-saturated ODT solution was passed for 1 h at 95 °C, then switching to neat solvent for washing.

2922–2921 cm^{-1} and 2852–2850 cm^{-1} taking a somewhat intermediate position between the frequency for crystalline-like (2918 and 2850 cm^{-1}) and liquid-like regions (2928 and 2858 cm^{-1}) [58,59].

For a more detailed and sensitive analysis of the band characteristics of ODT, time-resolved adsorption-desorption spectra were evaluated using 2D correlation analysis [66,67] and phase sensitive detection (PSD) in the framework of modulation excitation spectroscopy [68,69]. The changes were very small, but both analyses clearly showed that during the course of the adsorption the positions of the $\nu_{AS}(CH_2)$ and $\nu_S(CH_2)$ bands were blueshifted by 1–3 cm^{-1}, while to a similar extent redshifts were observed during the washing/desorption. Identical trends were observed under high H_2 pressure (50 bar), mimicking the hydrogenation condition (spectra are shown in electronic support information).

In the inset of Fig. 5, the adsorption and possible desorption behaviors of ODT on the Au catalysts under conditions similar to the ones of the oxidation reaction are shown. Obviously, ODT was hardly removed from the catalyst surface during rinsing with neat solvent. Notably, the integrated peak intensity was higher for the catalyst with the larger Au particle (6.9 nm) which has a smaller Au surface compared to the smaller Au particles.

Thermogravimetric desorption experiments (electronic support information) were conducted following the desorption of ODT from Au/TiO_2 after the preadsorption of ODT. They revealed a desorption temperature from Au/TiO_2 (2.1 nm) of ≈236 °C and of ≈276 °C from Au/TiO_2 (6.9 nm), indicating a higher stability of ODT on the larger particles.

Table 2
Summary of IR frequencies (in cm^{-1}) observed for various C–H stretching vibrations for ODT adsorbed on Au/TiO_2 (2.1 and 6.9 nm) and Au/CeO_2 (2.1 and 6.9 nm).

	Au/TiO_2		
	SAM on Au [71]	2.1 nm	6.9 nm
$\nu_{AS}(CH_3)$ ip	2965	2956[a]	2958[a]
$\nu_{AS}(CH_3)$ op	2958		
$\nu_{AS}(CH_2)$	2919	2922	2921
$\nu_S(CH_3)$	2873	2873	2873
$\nu_S(CH_2)$	2851	2852	2852
	Au/CeO_2		
	2.1 nm		6.9 nm
$\nu_{AS}(CH_3)$ ip	2956[a]		2956[a]
$\nu_{AS}(CH_3)$ op			
$\nu_{AS}(CH_2)$	2922		2922
$\nu_S(CH_3)$	2873		2873
$\nu_S(CH_2)$	2851		2852

[a] The observed band is likely resulting from the two overlapping bands.

3.5. Mercaptoacetic acid (MAA) adsorption

Mercaptoacetic acid (MAA) possesses two possible adsorption sites: a carboxylic and a thiol group. The appearance of the valence stretching mode of the thiol group (ν(S-H)) expected at around 2600–2500 cm^{-1} [70] is an indicator whether the thiol has undergone S-H scission upon adsorption on Au via the thiol group [64,71] or whether the molecule binds via its carboxylic group to the gold surface. This assumption also holds for a hypothetical "chelating" adsorption of MAA on the Au particles via the thiol *and* the carboxylic group which has been shown to be a possible adsorption mode for mercapto-carboxylic acids like glutathione on Au surfaces [72,73].

Similar to the ODT adsorption experiments, 1 mM MAA solution was passed over the catalysts and TiO_2 support for 1 h. The resulting IR spectra after the MAA adsorption on (A) TiO_2 support, (B) Au/TiO_2 (6.9 nm), and (C) Au/TiO_2 (2.1 nm) are shown in Fig. 6. Contrary to the weak interaction of ODT with the support, MAA showed strong interaction and adsorption on the TiO_2 support. The bands that originate from the adsorption of MAA on TiO_2 via the carboxylic group appear at ca. 1690, 1543, 1421 and 1392 cm^{-1}, in good agreement to the reported C=O vibrational frequency values for carboxylic acids on TiO_2 (1700–1200 cm^{-1}) [74,75]. The band intensities were significantly stronger than for the Au supported catalysts. The ν(S-H), which was more pronounced on the bare TiO_2, is located at 2550 cm^{-1}, showing minor cleavage of the S–H bond upon MAA adsorption on TiO_2. Subtraction of the support adsorption components (Fig. 6A) from the IR spectra of MAA on Au catalysts (Fig. 6B and C) indicated that MAA, upon adsorption on the Au particles, shows a prominent carbonyl stretching ν(C=O) band at ≈1702 cm^{-1}, while the intensity of the ν(S–H) band was negligible. Also, the ratio between ν(S–H) and ν(C=O) decreased with increasing Au surface area: the pure support shows ν(S–H)/ν(C=O) value of 0.41, Au/TiO_2 (6.9 nm) exhibits a ratio of 0.075 while the sample with the largest Au area (see Section 2), Au/TiO_2 (2.1 nm) shows even a lower value of 0.068. These observations clearly indicate the adsorption of MAA on the Au particles via the S atom in the thiolate form. The vibrational spectra observed at higher temperature (95 °C) under similar conditions to the oxidation reaction showed the same spectral features as those recorded at room temperature. Mimicking the hydrogenation reaction condition by applying 50 bar H_2 did not alter the ν(S-H) and ν(C=O) signal positions but resulted in spectral changes in the carbonate region. These results suggest a strong adsorption of MAA under the oxidation and hydrogenation conditions in the absence of substrate. Due to the surprisingly moderate poisoning effect of MAA on the oxidation of benzyl alcohol (Fig. 1B), the adsorption–desorption behavior of MAA under the oxidation reaction condition in the presence of benzyl alcohol was investigated. The ν(C=O) band area, characteristic of MAA adsorption on Au, was monitored during *in situ* ATR-IR transient experiments (Fig. 6, right) where the solutions of MAA and benzyl alcohol were admitted alternately to the measurement cell. Remarkably, a large amount, about 30%, of MAA was removed from the Au surface when the MAA solution had been replaced by a solution of benzyl alcohol. This behavior, i.e. the competitive adsorption, was reversible.

Table 3
Binding energies of MAA on the Au_{37} cluster obtained by the DFT calculations.

Adsorption geometry Fig. 7	Binding energy (kJ/mol)	Binding energy (kJ/mol) – BSSE corrected
A—Au (1 1 1)	157.7	135.4
B—Au (1 0 0)	164.9	140.5
C—Au (1 1 1), no corners	135.1	115.1
D—edge	206.4	177.3
E—corner	192.2	119.0

Thermogravimetric desorption studies revealed a desorption temperature of ≈180–220 °C from Au/TiO_2 (2.1 nm) and of ≈169 °C from Au/TiO_2 (6.9 nm), indicating a more stable MAA adsorption on smaller Au particles (electronic support information).

To gain further insight into the nature of MAA adsorption on Au particles DFT calculations were performed. As evidenced from the IR experiments, the thiol group was set to be in a deprotonated form. Five distinct adsorption sites were considered using the same Au cluster (Fig. 7A–E): (i) a small (1 1 1) surface with the spread of 6 Au atoms, (ii) a small (1 0 0) surface with the spread of 9 Au atoms, (iii) a larger (1 1 1) surface with the spread of 19 Au atoms, (iv) an edge site between (i) and (ii), and (v) a corner site between (i) and (ii). Atop thiolate adsorption modes were taken as the initial configuration and the resulting optimized structures are depicted in Fig. 7A–E. The corresponding binding energies are given in Table 3. The BSSE corrected binding energies are also shown for the sake of complete comparisons; however it should be noted that the thiolate adsorption forms a 'chemical' bond with Au. Therefore the BSSE correction can be greatly biased by the homolytic cleavage energy of the Au-S bond and does not likely result in the correct evaluation of the interaction energies. For this reason, the MAA adsorption strength is discussed based on the BSSE uncorrected adsorption energies.

Clearly, MAA thiolate binds more strongly onto the defect sites than on the (1 1 1) and (1 0 0) facets, showing twofold but different binding modes on the edge and corner. The most stable adsorption mode is via the twofold Au-S binding on the edge (Fig. 7D), while

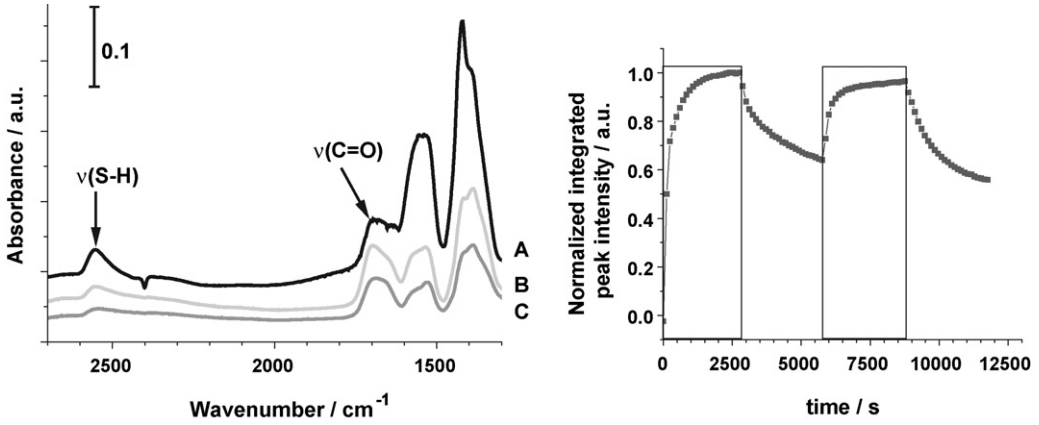

Fig. 6. Left: ATR-IR spectra recorded after passing a 1 mM solution of MAA for 1 h over TiO_2 (A, black line), Au/TiO_2 (6.9 nm) (light gray, B), and Au/TiO_2 (2.1 nm) (gray, C). Right: Integrated peak intensity of the ν(C=O) due to MAA during switching between the two flows of O_2-saturated 1 mM solution of MAA in toluene (marked by rectangles) and O_2-saturated 10 mM solution of benzyl alcohol in toluene at 95 °C. The catalyst studied was Au/TiO_2 (2.1 nm).

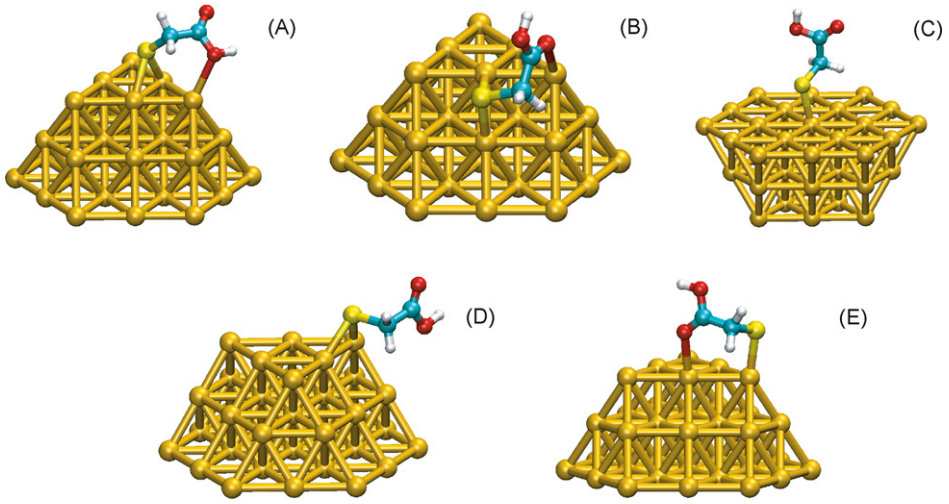

Fig. 7. Energetic minimum configurations of MAA adsorbed on the Au(1 1 1) (A), the Au(1 0 0) part of the particle (B), larger Au(1 1 1) facets (C), and adsorbed on two corner/edge positions in a twofold binding geometry through the thiolate group (D) and a chelate configuration involving a binding through the thiolate and the carboxylic group (E). (For interpretation of the references to colour in this figure legend, the reader is referred to the web version of this article.)

the second most stable mode involves both thiolate and carboxylic groups via one Au(edge)-S and one Au(corner)-O, both atop, bindings (Fig. 7E). The MAA binding modes on (i, Fig. 7A) and (ii, Fig. 7B) sites were similar, both involving twofold Au-S bonds and one-fold Au–O bond at the corner site. The least stable one was on the large terrace of (1 1 1) surface via atop one-fold Au–S bond without an Au-carboxylic group interaction. In all the investigated cases, the carboxylic group interacted exclusively with the defect sites.

4. Discussion

4.1. Adsorption of thiols

The dynamics of thiol layer formation on the Au particles was studied by time-resolved ATR-IR spectroscopy, PSD and 2D Correlation Analysis (electronic support information) showing a blueshift in the position of the $\nu_{AS}(CH_2)$ and $\nu_S(CH_2)$ signals during the course of ODT adsorption. This indicates that at first a rather crystalline-like layer is formed, corresponding to adsorption on Au crystal facets. After the occupation of these sites, ODT binds in a way that leads to the formation of a more liquid-like layer. This liquid-like layer formation was reported for small Au particles [64,76] resulting from the occupation of a higher fraction of low coordinated sites. Additionally, the desorption temperature in the thermogravimetric desorption experiments was found to be higher on the larger particles. This may be related to the intensity of the IR bands which was higher in the systems containing larger particles (6.9 nm) despite the much higher Au area of the small (2.1 nm) Au particles. A very small fraction of the adsorbed ODT is bound reversibly as shown by the decreasing intensity of $\nu_{AS}(CH_2)$ and $\nu_S(CH_2)$ during rinsing with neat solvent (inset Fig. 5). On the contrary, theoretical calculations have shown that thiols bound to these low coordinated Au sites show a higher adsorption energy [64,65]; however they are exchanged faster [57,76–79] presumably due to a strong steric hindrance within well-ordered, crystalline-like layers that are formed on extended Au surfaces.

The adsorption of the bifunctional thiol MAA is more complex compared to ODT. The adsorption of MAA on Au should require a breakage of the S-H bond whereas its adsorption on the support via the carboxylic group likely leaves the S—H bond intact. Desorption experiments showed that MAA desorbs at lower temperatures compared to ODT (thermogravimetric desorption experiments, electronic support information). Particularly, MAA desorbs at lower temperatures from the larger particles contrary to ODT which has a higher thermal stability on the larger particles. DFT calculations were performed using a model cluster containing multiple adsorption sites, e.g. Au(1 0 0) and Au(1 1 1) surface facets as well as edges and corner sites. According to the DFT calculations the most preferred adsorption site of MAA on the cluster is the edge site formed at the boundary of the (1 1 1) and (1 0 0) facets via a twofold Au—S bond formation (Fig. 7D). Au–S adsorption of MAA thiolate at the corner site involves a second interaction of the carboxylic group with the edge site (Fig. 7E), which shows slightly less but significant binding to the Au cluster. The adsorption modes on the small (1 1 1) and (1 0 0) surfaces (Fig. 7A and B), via twofold Au–S and carboxylic oxygen–Au edge sites interactions, as well as on the larger (1 1 1) terrace via one-fold Au–S interaction (Fig. 7C) were considerably less stable than the edge and corner adsorption modes. The adsorption energies of MAA were found to be in good agreement with energies observed for thiols/thiolates adsorbed on Au ([80,81] and references therein). These two most stable configurations (Table 3) possibly explain the major loss of activity in the hydrogenation of ketopantolactone when MAA is added as a poisoning agent.

4.2. Electron microscopy, ball model

Two probable models for the morphology of the Au particles were identified by means of TEM (Fig. 3). Selected relative contributions of special surface sites can be estimated using the formulas given in [34,35]. However, we cannot exclude the possibility of adsorbate (reactants, poisons, solvent) induced surface reconstruction [82–84]. A flexible, dynamic particle model [85,86] could be considered rather than the rigid one following the idealized van Hardeveld calculations discussed here.

In particular the models chosen here reveal an influence of particle diameter and thickness on the relative number of edge and corner sites. Assuming a flat cuboctahedron particle (Fig. 4A), we calculate that a particle with a diameter of 2.1 nm has a factor of 6.3 higher amount of edge and corner atoms compared to a particle of 6.9 nm diameter. Using a truncated tetrahedron model (Fig. 4B) we obtain a value of 5.9.

4.3. Catalysis

A drop in conversion with increasing Au particle size was observed in the hydrogenation of ketopantolactone. The activity of the Au/TiO_2 (2.1 nm) was approximately 4 times higher (Table 1)

compared to the Au/TiO_2 (6.9 nm), which is in fairly good agreement to the decrease in the relative amount of corner and edge sites with increasing particle size (see above). The addition of a large amount of ODT as a poisoning (blocking) agent during the hydrogenation reaction did not lead to a total loss of activity. The results obtained from *in situ* ATR-IR spectroscopy indicated that ODT preferentially forms rather ordered layers typical for crystal facets in the first stage of adsorption, and the more dynamic and exchangeable ODT molecules exhibit or induce a rather liquid-like structure, typical for the adsorption on edges, corners or highly rounded surfaces (Table 2, Fig. 5). The addition of 10 mol% MAA/Au_{Total} to the hydrogenation mixture quickly led to a strong loss of catalytic activity by blocking the active sites for hydrogenation (Fig. 2B). It has been proposed that edge and corner sites of supported Au particles are the main active species in hydrogenation of the C=O bond [53,55,87], and the present poisoning studies support these findings.

On the other hand, in the aerobic oxidation of benzyl alcohol the addition of 10 mol% ODT/Au_{Total} led to an almost complete blocking of the active sites (Fig. 1A). In contrast to the behavior of ODT, the addition of MAA resulted in a mild loss of the oxidation activity (Fig. 1B) even when the added amount was significantly larger than the one necessary to cover the whole Au surface.

The contrasting poisoning effects of ODT and MAA in the tested oxidation and hydrogenation reactions are striking. A possible interpretation to these macroscopically observed phenomena lies in selective site-blocking [88] of catalytic sites. A selective site-blocking pattern occurs when the inhibitor is preferentially bound to the most active sites and leads to a specific site blocking which causes a deactivation of the catalyst even when only small amounts of the poison are added.

The alcohol oxidation likely requires certain active sites on Au nanoparticles which can be generated by the removal of MAA from the surface. The competitive adsorption between MAA and benzyl alcohol under reaction conditions was confirmed by means of *in situ* ATR-IR experiments for MAA (inset Fig. 6). Note that also short-chain thiols and short chain ($n < 2$) ω-SH carboxylic acids exhibit a distinctly smaller peak potential for the reductive desorption from Au electrodes. This effect has been assigned to the inability of these short-chain molecules to form highly ordered, stable layers [89]. Our thermogravimetric desorption experiments also showed higher stability of MAA on smaller Au particles.

In contrast, apparently ODT is not removed by the competitive adsorption from the active site for the oxidation of benzyl alcohol – already the addition of a small portion leads to total deactivation (Fig. 1). ODT is suggested to form ordered layers strongly bound to the exposed crystal facets (Table 2, Fig. 5). The thermogravimetric desorption experiments indicated that ODT exhibits higher stability on larger Au particles. This is in line with stable ODT layer formation on the large crystal facets and the DFT results for MAA on the Au cluster, i.e. stronger adsorption on edge and corner sites.

Finally, it should be stressed that an absolute assessment of the active Au sites in the oxidation of benzyl alcohol and the hydrogenation of ketopantolactone cannot be made without considering the effect of the site-blocking on the adsorption of oxygen and hydrogen. This aspect which has not been elucidated in the present work needs attention before the observed structure sensitivity can be explained profoundly. Although it has been shown that both oxygen and hydrogen are dissociatively adsorbed and suggestions have been made where these adsorptions occur preferentially [9,13,14,90], this information is not sufficient for a thorough understanding of the observed structure sensitivity and further experimental work is required.

To sum up, the findings presented here strongly point to a different nature of the active Au sites for the oxidation of benzyl alcohols and the hydrogenation of ketopantolactone. The knowledge gained from the selective poisoning of gold catalysts by thiols may assist in understanding and improving this type of catalysts for selective oxidation and hydrogenation reactions.

5. Conclusions

Oxidation of benzyl alcohol and hydrogenation of ketopantolactone has been studied on TiO_2 and CeO_2 supported gold catalysts with different Au particle size (2.1 and 6.9 nm) in the presence and absence of poisoning (blocking) thiols (n-octadecanethiol (ODT) and mercaptoacetic acid (MAA)). The effect of the adsorption of the two thiols with different functional groups on the catalytic behavior of the gold catalysts has been investigated. Upon addition of 10 mol% $thiol/Au_{Total}$, an almost complete loss of activity in the aerobic oxidation of benzyl alcohol was observed when the Au catalysts were poisoned by ODT, while at the same concentration MAA adsorption had relatively little influence on activity. In contrast, in the hydrogenation of ketopantolactone similar blocking (10 mol% $thiol/Au_{Total}$) with MAA led to a strong loss in activity, while ODT adsorption affected the activity relatively little. The nature of ODT and MAA adsorptions on the Au catalysts was investigated by means of *in situ* ATR-IR spectroscopy, thermogravimetric desorption and DFT calculations. During the course of adsorption, ODT first binds to crystal facets of the Au particles and later forms reversibly bound species on the surface, likely adsorbing on edge and corner sites. On the other hand, MAA strongly binds to the edge and corner sites on the supported Au clusters as indicated by DFT calculations. The adsorption of MAA on crystal facets is thermodynamically the least stable configuration. The stronger adsorption on large Au terraces for ODT and on defect sites such as crystal edge and corner for MAA are also confirmed by desorption experiments, showing higher stability of ODT on the larger and MAA on the smaller Au particles, respectively. *In situ* ATR-IR experiments under reaction conditions showed that MAA can be partially removed from the Au surface by the substrate used in the oxidation, benzyl alcohol, which likely led to the active site generation for the oxidation reaction. These results suggest that the hydrogenation reaction is catalyzed by mainly low-coordinated Au atoms such as edges and corners and the active sites can be efficiently blocked by MAA. In contrast, the oxidation reaction seems to prevail on extended Au faces which can be effectively poisoned by strong ODT adsorption. These findings show that different active sites are involved in aerobic oxidation of benzyl alcohol and the hydrogenation of ketopantolactone and underline the importance of a structural tailoring of the active gold particles for a specific reaction.

Acknowledgements

We thank Frank Krumeich for the electron microscopy investigations performed at the electron microscopy center of ETH Zurich (EMEZ). P.H. thanks Daniel M. Meier for fruitful comments about MAA.

Appendix A. Supplementary data

Supplementary data associated with this article can be found, in the online version, at doi:10.1016/j.molcata.2009.02.025.

References

[1] M. Haruta, Chem. Rec. 3 (2003) 75–87.
[2] M. Haruta, Cattech 6 (2002) 102–115.
[3] G.C. Bond, D.T. Thompson, Cat. Rev.: Sci. Eng. 41 (1999) 319–388.
[4] M.C. Daniel, D. Astruc, Chem. Rev. 104 (2004) 293–346.
[5] A.S.K. Hashmi, G.J. Hutchings, Angew. Chem. Int. Ed. 45 (2006) 7896–7936.
[6] S. Chretien, S.K. Buratto, H. Metiu, Curr. Opin. Solid State Mater. Sci. 11 (2007) 62–75.

[7] C. Della Pina, E. Falletta, L. Prati, M. Rossi, Chem. Soc. Rev. 37 (2008) 2077–2095.
[8] M. Haruta, Catal. Today 36 (1997) 153–166.
[9] N. Lopez, T.V.W. Janssens, B.S. Clausen, Y. Xu, M. Mavrikakis, T. Bligaard, J.K. Nørskov, J. Catal. 223 (2004) 232–235.
[10] M. Mavrikakis, P. Stoltze, J.K. Nørskov, Catal. Lett. 64 (2000) 101–106.
[11] I.N. Remediakis, N. Lopez, J.K. Nørskov, Appl. Catal. A: Gen. 291 (2005) 13–20.
[12] R. Grisel, K.J. Weststrate, A. Gluhoi, B.E. Nieuwenhuys, Gold Bull. 35 (2002) 39–45.
[13] B. Yoon, H. Hakkinen, U. Landman, A.S. Worz, J.M. Antonietti, S. Abbet, K. Judai, U. Heiz, Science 307 (2005) 403–407.
[14] B. Hvolbæk, T.V.W. Janssens, B.S. Clausen, H. Falsig, C.H. Christensen, J.K. Nørskov, Nano Today 2 (2007) 14–18.
[15] Z.P. Liu, P. Hu, A. Alavi, J. Am. Chem. Soc. 124 (2002) 14770–14779.
[16] G. Mills, M.S. Gordon, H. Metiu, J. Chem. Phys. 118 (2003) 4198–4205.
[17] B.L. Zhu, R.J. Angelici, J. Am. Chem. Soc. 128 (2006) 14460–14461.
[18] B.L. Zhu, R.J. Angelici, Chem. Commun. 21 (2007) 2157–2159.
[19] M. Turner, O.P.H. Vaughan, R.M. Lambert, Chem. Commun. 20 (2008) 2316–2318.
[20] L. Prati, F. Porta, Appl. Catal. A: Gen. 291 (2005) 199–203.
[21] L. Prati, M. Rossi, J. Catal. 176 (1998) 552–560.
[22] S. Biella, F. Porta, L. Prati, M. Rossi, Catal. Lett. 90 (2003) 23–29.
[23] S. Carrettin, P. McMorn, P. Johnston, K. Griffin, C.J. Kiely, G.A. Attard, G.J. Hutchings, Top. Catal. 27 (2004) 131–136.
[24] N. Dimitratos, J.A. Lopez-Sanchez, D. Morgan, A. Carley, L. Prati, G.J. Hutchings, Catal. Today 122 (2007) 317–324.
[25] V.R. Choudhary, A. Dhar, P. Jana, R. Jha, B.S. Uphade, Green Chem. 7 (2005) 768–770.
[26] W.C. Ketchie, Y.L. Fang, M.S. Wong, M. Murayama, R.J. Davis, J. Catal. 250 (2007) 94–101.
[27] P. Haider, J.-D. Grunwaldt, A. Baiker, Catal. Today In Press, Corrected Proof, doi:10.1016/j.cattod.2008.06.003 (2008).
[28] P. Haider, B. Kimmerle, F. Krumeich, W. Kleist, J.D. Grunwaldt, A. Baiker, Catal. Lett. 125 (2008) 169–176.
[29] K.-Q. Sun, S.-W. Luo, N. Xu, B.-Q. Xu, Catal. Lett. 124 (2008) 238–242.
[30] S. Carrettin, P. McMorn, P. Johnston, K. Griffin, C.J. Kiely, G.J. Hutchings, PCCP 5 (2003) 1329–1336.
[31] F. Porta, L. Prati, M. Rossi, S. Coluccia, G. Martra, Catal. Today 61 (2000) 165–172.
[32] K. Lehnert, P. Claus, Catal. Commun. 9 (2008) 2543–2546.
[33] J. Chen, Q. Zhang, Y. Wang, H. Wan, Adv. Synth. Catal. 350 (2008) 453–464.
[34] R. Van Hardeveld, A. Van Montfoort, Surf. Sci. 4 (1966) 396–430.
[35] R. Van Hardeveld, F. Hartog, Surf. Sci. 15 (1969) 189–230.
[36] G. Ertl, Cat. Rev.: Sci. Eng. 21 (1980) 201–223.
[37] G. Ertl, Surf. Sci. 300 (1994) 742–754.
[38] G. Ertl, J. Mol. Cat. A: Chem. 182–183 (2002) 5–16.
[39] G.A. Somorjai, Acc. Chem. Res. 9 (1976) 248–256.
[40] X.Y. Deng, B.K. Min, A. Guloy, C.M. Friend, J. Am. Chem. Soc. 127 (2005) 9267–9270.
[41] W.W. Gao, L. Zhou, D.S. Pinnaduwage, C.M. Friend, J. Phys. Chem. C 111 (2007) 9005–9007.
[42] D.G. Duff, A. Baiker, P.P. Edwards, Langmuir 9 (1993) 2301–2309.
[43] J.D. Grunwaldt, C. Kiener, C. Wögerbauer, A. Baiker, J. Catal. 181 (1999) 223–232.
[44] A.A. Herzing, C.J. Kiely, A.F. Carley, P. Landon, G.J. Hutchings, Science 321 (2008) 1331–1335.
[45] A. Urakawa, R. Wirz, T. Bürgi, A. Baiker, J. Phys. Chem. B 107 (2003) 13061–13068.
[46] A.D. Becke, J. Chem. Phys. 98 (1993) 5648–5652.
[47] J.P. Perdew, Y. Wang, Phys. Rev. B 45 (1992) 13244–13249.
[48] M.J. Frisch, G.W. Trucks, H.B. Schlegel, G.E. Scuseria, M.A. Robb, J.R. Cheeseman, J.A. Montgomery Jr., T. Vreven, K.N. Kudin, J.C. Burant, J.M. Millam, S.S. Iyengar, J. Tomasi, V. Barone, B. Mennucci, M. Cossi, G. Scalmani, N. Rega, G.A. Petersson, H. Nakatsuji, M. Hada, M. Ehara, K. Toyota, R. Fukuda, J. Hasegawa, M. Ishida, T. Nakajima, Y. Honda, O. Kitao, H. Nakai, M. Klene, X. Li, J.E. Knox, H.P. Hratchian, J.B. Cross, C. Adamo, J. Jaramillo, R. Gomperts, R.E. Stratmann, O. Yazyev, A.J. Austin, R. Cammi, C. Pomelli, J. Ochterski, P.Y. Ayala, K. Morokuma, G.A. Voth, P. Salvador, J.J. Dannenberg, V.G. Zakrzewski, S. Dapprich, A.D. Daniels, M.C. Strain, O. Farkas, D.K. Malick, A.D. Rabuck, K. Raghavachari, J.B. Foresman, J.V. Ortiz, Q. Cui, A.G. Baboul, S. Clifford, J. Cioslowski, B.B. Stefanov, G. Liu, A. Liashenko, P. Piskorz, I. Komaromi, R.L. Martin, D.J. Fox, T. Keith, M.A. Al-Laham, C.Y. Peng, A. Nanayakkara, M. Challacombe, P.M.W. Gill, B. Johnson, B. Chen, M.W. Wong, C. Gonzalez, J.A. Pople, GAUSSIAN 03 rev. C. 02, Gaussian Inc, Pittsburgh, PA, 2003.
[49] P.J. Hay, W.R. Wadt, J. Chem. Phys. 82 (1985) 299–310.
[50] S.F. Boys, F. Bernardi, Mol. Phys. 19 (1970) 553–566.
[51] A. Abad, P. Concepción, A. Corma, H. García, Angew. Chem. Int. Ed. 44 (2005) 4066–4069.
[52] D.I. Enache, D.W. Knight, G.J. Hutchings, Catal. Lett. 103 (2005) 43–52.
[53] C. Mohr, H. Hofmeister, P. Claus, J. Catal. 213 (2003) 86–94.
[54] C. Mohr, H. Hofmeister, J. Radnik, P. Claus, J. Am. Chem. Soc. 125 (2003) 1905–1911.
[55] R. Zanella, C. Louis, S. Giorgio, R. Touroude, J. Catal. 223 (2004) 328–339.
[56] J.E. Bailie, G.J. Hutchings, Chem. Commun. 21 (1999) 2151–2152.
[57] J.C. Love, L.A. Estroff, J.K. Kriebel, R.G. Nuzzo, G.M. Whitesides, Chem. Rev. 105 (2005) 1103–1169.
[58] P.E. Laibinis, G.M. Whitesides, D.L. Allara, Y.T. Tao, A.N. Parikh, R.G. Nuzzo, J. Am. Chem. Soc. 113 (1991) 7152–7167.
[59] L.H. Dubois, R.G. Nuzzo, Annu. Rev. Phys. Chem. 43 (1992) 437–463.
[60] M.D. Porter, T.B. Bright, D.L. Allara, C.E.D. Chidsey, J. Am. Chem. Soc. 109 (1987) 3559–3568.
[61] A. Badia, S. Singh, L. Demers, L. Cuccia, G.R. Brown, R.B. Lennox, Chem. Eur. J. 2 (1996) 359–363.
[62] D.A. Hutt, G.J. Leggett, J. Phys. Chem. 100 (1996) 6657–6662.
[63] Y.K. Kim, J.P. Koo, J.S. Ha, Appl. Surf. Sci. 249 (2005) 7–11.
[64] A.C. Templeton, M.P. Wuelfing, R.W. Murray, Acc. Chem. Res. 33 (2000) 27–36.
[65] W.D. Luedtke, U. Landman, J. Phys. Chem. B 102 (1998) 6566–6572.
[66] I. Noda, Appl. Spectrosc. 47 (1993) 1329–1336.
[67] I. Noda, Anal. Sci. 23 (2007) 139–146.
[68] D. Baurecht, U.P. Fringeli, Rev. Sci. Instrum. 72 (2001) 3782–3792.
[69] T. Bürgi, A. Baiker, Adv. Catal. 50 (2006) 227–283.
[70] D.W. Mayo, F.A. Miller, R.W. Hannah, Course Notes on the Interpretation of Infrared and Raman Spectra, John Wiley & Sons, Hoboken, New Jersey, 2003.
[71] R.G. Nuzzo, L.H. Dubois, D.L. Allara, J. Am. Chem. Soc. 112 (1990) 558–569.
[72] M. Bieri, T. Bürgi, Langmuir 21 (2005) 1354–1363.
[73] M. Bieri, T. Bürgi, PCCP 8 (2006) 513–520.
[74] A.M. Johnson, S. Trakhtenberg, A.S. Cannon, J.C. Warner, J. Phys. Chem. A 111 (2007) 8139–8146.
[75] Y.X. Weng, L. Li, Y. Liu, L. Wang, G.Z. Yang, J. Phys. Chem. B 107 (2003) 4356–4363.
[76] M.J. Hostetler, J.E. Wingate, C.J. Zhong, J.E. Harris, R.W. Vachet, M.R. Clark, J.D. Londono, S.J. Green, J.J. Stokes, G.D. Wignall, G.L. Glish, M.D. Porter, N.D. Evans, R.W. Murray, Langmuir 14 (1998) 17–30.
[77] C.E.D. Chidsey, C.R. Bertozzi, T.M. Putvinski, A.M. Mujsce, J. Am. Chem. Soc. 112 (1990) 4301–4306.
[78] M.J. Hostetler, A.C. Templeton, R.W. Murray, Langmuir 15 (1999) 3782–3789.
[79] C. Binet, M. Daturi, J.C. Lavalley, Catal. Today 50 (1999) 207–225.
[80] M.J. Esplandiu, M.L. Carot, F.P. Cometto, V.A. Macagno, E.M. Patrito, Surf. Sci. 600 (2006) 155–172.
[81] C. Masens, M.J. Ford, M.B. Cortie, Surf. Sci. 580 (2005) 19–29.
[82] G.A. Somorjai, THEOCHEM 424 (1998) 101–117.
[83] T. Diemant, Z. Zhao, H. Rauscher, J. Bansmann, R. Behm, Top. Catal. 44 (2007) 83–93.
[84] S.M. Driver, T.F. Zhang, D.A. King, Angew. Chem. Int. Ed. 46 (2007) 700–703.
[85] L.D. Marks, Rep. Prog. Phys. 57 (1994) 603–649.
[86] C.L. Kuo, P. Clancy, J. Phys. Chem. B 109 (2005) 13743–13754.
[87] E. Bus, R. Prins, J.A. van Bokhoven, Catal. Commun. 8 (2007) 1397–1402.
[88] C.H. Bartholomew, Appl. Catal. A: Gen. 212 (2001) 17–60.
[89] S. Imabayashi, M. Iida, D. Hobara, Z.Q. Feng, K. Niki, T. Kakiuchi, J. Electroanal. Chem. 428 (1997) 33–38.
[90] L. Barrio, P. Liu, J.A. Rodriguez, J.M. Campos-Martin, J.L.G. Fierro, J. Chem. Phys. 125 (2006) 164715.